




Article

Synthesis and Biological Activity Evaluations of Green ZnO-Decorated Acid-Activated Bentonite-Mediated Curcumin Extract (ZnO@CU/BE) as Antioxidant and Antidiabetic Agents

Hassan Ahmed Rudayni ¹, Marwa H. Shemy ^{2,3}, Malak Aladwani ¹, Lina M. Alneghery ¹,
Gasem M. Abu-Taweel ⁴, Ahmed A. Allam ⁵, Mostafa R. Abukhadra ^{3,6,*} and Stefano Bellucci ^{7,*}

¹ Department of Biology, College of Science, Imam Muhammad bin Saud Islamic University, Riyadh 11623, Saudi Arabia

² Chemistry Department, Faculty of Science, Beni-Suef University, Beni-Suef 65211, Egypt

³ Materials Technologies and Their Applications Lab, Geology Department, Faculty of Science, Beni-Suef University, Beni-Suef 65214, Egypt

⁴ Department of Biology, College of Science, Jazan University, P.O. Box 2079, Jazan 45142, Saudi Arabia

⁵ Zoology Department, Faculty of Science, Beni-Suef University, Beni-Suef 62514, Egypt

⁶ Geology Department, Faculty of Science, Beni-Suef University, Beni-Suef 65214, Egypt

⁷ INFN-Laboratori Nazionali di Frascati, Via. E. Fermi 54, 00044 Frascati, Italy

* Correspondence: abukhadra89@science.bsu.edu.eg (M.R.A.); stefano.bellucci@inf.infn.it (S.B.)

Abstract: Green ZnO-decorated acid-activated bentonite-mediated curcumin extract (ZnO@CU/BE) was prepared as a multifunctional antioxidant and antidiabetic agent based on the extract of curcumin, which was used as a reducing and capping reagent. ZnO@CU/BE showed notably enhanced antioxidant properties against nitric oxide ($88.6 \pm 1.58\%$), 1,1-diphenyl-2-picrylhydrazil ($90.2 \pm 1.76\%$), 2,2'-azino-bis(3-ethylbenzothiazoline-6-sulphonic acid ($87.3 \pm 1.61\%$), and superoxide ($39.5 \pm 1.12\%$) radicals. These percentages are higher than the reported values of ascorbic acid as a standard and the integrated components of the structure (CU, BE/CU, and ZnO). This signifies the impact of the bentonite substrate on enhancing the solubility, stability, dispersion, and release rate of the intercalated curcumin-based phytochemicals, in addition to enhancing the exposure interface of ZnO nanoparticles. Therefore, effective antidiabetic properties were observed, with significant inhibition effects on porcine pancreatic α -amylase ($76.8 \pm 1.87\%$), murine pancreatic α -amylase ($56.5 \pm 1.67\%$), pancreatic α -glucosidase ($96.5 \pm 1.07\%$), murine intestinal α -glucosidase ($92.5 \pm 1.10\%$), and amyloglucosidase ($93.7 \pm 1.55\%$) enzymes. These values are higher than those determined using commercial miglitol and are close to the values measured using acarbose. Hence, the structure can be applied as an antioxidant and antidiabetic agent.

Keywords: bentonite; ZnO; curcumin; composite; antioxidant; antidiabetes



Citation: Rudayni, H.A.; Shemy, M.H.; Aladwani, M.; Alneghery, L.M.; Abu-Taweel, G.M.; Allam, A.A.; Abukhadra, M.R.; Bellucci, S. Synthesis and Biological Activity Evaluations of Green ZnO-Decorated Acid-Activated Bentonite-Mediated Curcumin Extract (ZnO@CU/BE) as Antioxidant and Antidiabetic Agents. *J. Funct. Biomater.* **2023**, *14*, 198. <https://doi.org/10.3390/jfb14040198>

Academic Editor: Nenad Ignjatovic

Received: 19 January 2023

Revised: 1 March 2023

Accepted: 7 March 2023

Published: 4 April 2023



Copyright: © 2023 by the authors. Licensee MDPI, Basel, Switzerland. This article is an open access article distributed under the terms and conditions of the Creative Commons Attribution (CC BY) license (<https://creativecommons.org/licenses/by/4.0/>).

1. Introduction

Diabetes is a widely distributed clinical pancreatic syndrome whose symptoms eventually increase in subsequent periods and is predicted to be the seventh leading cause of mortality. According to the World Health Organization (WHO), 366 million individuals will be diagnosed by 2030 [1–3]. Diabetes is classified into type 1 diabetes mellitus (T1DM) and type 2 diabetes mellitus (T2DM), which will represent 90% of patients with diabetes by 2030 [1,4]. T2DM is a severe metabolic disorder associated with postprandial hyperglycemia (significant levels of glucose) and abnormal elevation of the levels of released free radicals (reactive oxygen) [5–7]. The hyperglycemia and the increase in blood glucose concentrations are affected mainly by the levels of the generated oxidative enzymes such as α -amylase, α -glucosidase, and amyloglucosidase enzymes. Such enzymes accelerate strongly the breakdown reactions of complex sugars into glucose and its absorption rate [5,7]. Chronic hyperglycemia causes a significant increase in the production of

advanced glycation products (AGEs) that significantly affect the pathogenesis associated with diabetic complications [8,9]. The release of the reactive oxygen species results in the development of pathophysiological conditions involving the weakening of antioxidant defense mechanisms [7,10,11]. Additionally, oxidative stress is an essential factor involved in inducing insulin resistance, lipid peroxidation, and the destruction of cellular organelles and blood vessels [8,9,12].

Several chemical antidiabetic drugs (biguanides, miglitol, sulfonylureas, acarbose, thiazolidinedione, and voglibose) have been used effectively to reduce hyperglycemia and oxidizing radicals [7,9]. However, they do not exhibit adequate long-term effects and are associated with adverse health issues such as abdominal distention, diarrhea, hepatotoxicity, meteorism, and severe hypoglycemia [13,14]. Therefore, several studies have been conducted to design multifunctional structures with significant antioxidant and antidiabetic properties, strong preventive effects on the generation of oxidative stress, and the ability to manage T2DM [7,15]. Recently, metal and metal oxide nanostructures have been extensively investigated for this purpose owing to their reported biological activities, surface area, and physicochemical properties [15–17]. Moreover, they exhibit significant therapeutic and theranostic potentiality in addition to their remarkable safe effects on healthy cells and tissues [16,18]. Numerous edible plant species have been categorized as antioxidant and antidiabetic-safe products [9,15,19]. This is related to their phytochemical constituents (polyphenols, tannins, glucosinolates, terpenes, steroids, and carotenoids), which can reduce the level of sugar in the blood as well as the commonly reported risks of T2DM and its complications [10,20,21].

Zinc oxide and its nanomaterials have been reported as promising, safe, biocompatible, and non-toxic antidiabetic and antioxidant agents that exhibit notable preventive effects on the generation of free radicals [17,22,23]. Zinc is an essential and vital element in human organs and plays a significant role in the synthesis of nucleic acids and proteins [16,23,24]. Moreover, it is widely used in biomedical applications such as tissue engineering and drug delivery and in the development of antioxidant, antibacterial, anticancer, and hypoglycemic agents [16,25]. Recent studies have demonstrated the significant effects of synthesis methods, mechanical stability, morphology, hybridization, and surface modification of zinc oxide-based materials on their biomedical properties [16,17,26]. Moreover, the formation of complexes between zinc-based structures and common phytochemical compounds or their synthesis using plant-associated methods confers biocompatibility, genotoxicity, and antioxidant properties to the compounds [22,23,27,28]. Therefore, the green synthesis of zinc oxide based on extracts of plants, which are enriched with well-known antioxidant phytochemicals, such as *turmeric rhizome*, may lead to compounds with significant antidiabetic properties. Green synthesis methods have been widely recommended over the last decade as ecofriendly, cost-effective, simple, nontoxic, biosafe, and highly productive synthesis methods for nonagglomerated nanoparticles [17,29]. Moreover, the resulting particles are commonly coated with capping films of valuable phytochemicals, such as alkaloids, phenolic compounds, amino acids, and proteins [17].

Curcumin (CU) is a natural polyphenolic compound of low molecular weight extracted from *turmeric rhizome* (*Curcuma longa*). Curcumin is a potent natural antibacterial, antioxidant, antitumor, anti-inflammatory, and anticancer agent [27,30]. However, medical applications of curcumin are limited because of its low chemical stability, low water solubility, poor bioavailability, and fast metabolism properties [17,31,32]. Recent studies have demonstrated significant enhancement upon incorporation of curcumin into suitable carriers, as well as its conjugation with metal and metal oxides on its solubility and bioactivity as an antioxidant, anti-inflammatory, and antimicrobial agents [33–35]. The application of natural bentonite as a substrate for zinc oxide and zinc/curcumin complex, as well as a host for curcumin, will result in an innovative and enhanced multifunctional antioxidant and antidiabetic agent [24]. Bentonite is a common natural biocompatible clay mineral widely used in numerous pharmaceutical and medical applications and in drug delivery

systems [36–38] owing to its notable natural availability, high surface area, ion exchange capacity, adsorption and absorption properties, surface reactivity, and nontoxicity [36,39].

Therefore, the presented study aimed to synthesize ZnO-decorated bentonite-mediated curcumin extract (ZnO@CU/BE) by facile organic intercalation of the curcumin extract followed by green decoration of ZnO using the same curcumin extract as the reducing and capping reagent. The synesthetic composite was characterized as enhanced multifunctional antioxidant and antidiabetic agents with several species of bioactive compounds (curcumin-based phytochemicals, zinc oxide-capped curcumin, and zinc/curcumin complexes).

2. Materials and Methods

2.1. Materials and Chemicals

The raw bentonite sample used during the preparation of the structure was obtained from a bentonite quarry in Western Desert, Egypt with 54.82% (SiO₂), 17.56% (Al₂O₃), 9.5% (Fe₂O₃), 2.6% (Na₂O), 2.5% (MgO), 2.4% (CaO), 1.45% (TiO₂), and 9.2% (LOI). The acid activation step of bentonite occurred using sulfuric acid (99% purity; Sigma-Aldrich, Cairo city, Egypt). Highly pure curcumin (>94.99; Sigma-Aldrich) and analytical-grade absolute ethanol were used to obtain the green reducing extract and curcumin solution. Zinc nitrate hexahydrate (Zn(NO₃)₂·6H₂O) powder (98%; Sigma-Aldrich) salt is the incorporated precursor during the green support of ZnO nanoparticles into the bentonite carrier. α -amylase (EC Number: 232-565-6; CAS Number: 0009000902; Enzyme Commission number: 3.2.1.1 (BRENDA, IUBMB)), α -glucosidase (EC Number: 232-604-7; CAS Number: 9001-42-7; Enzyme Commission number: 3.2.1.20 (BRENDA, IUBMB)), amyloglucosidase (EC Number: 232-877-2; CAS Number: 9032-08-0; Enzyme Commission number: 3.2.1.3 (BRENDA, IUBMB)), Miglitol drug (C₈H₁₇NO₅), acarbose drug (\geq 95%; C₂₅H₄₃NO₁₈), para-nitrophenyl α -glucopyranoside (pNPG), glacial acetic acid, starch, ethylene diamine tetra acetic acid (EDTA), L-ascorbic acid, potassium persulfate, sodium nitroprusside, sulphanic acid, nitroblue tetrazolium (NBT), 1,1-diphenyl-2-picrylhydrazil (DPPH), 2,2'-azino-bis(3-ethylbenzothiazoline-6-sulphonic acid (ABTS), *N*-(1-Naphthyl) ethylenediamine dihydrochloride, and phosphate buffer were delivered from Sigma-Aldrich, Egypt and were used in the antioxidant and antidiabetic tests.

2.2. Synthesis of ZnO Decorated Acid Activated Bentonite Mediated Curcumin Extract (ZnO@CU/BE)

2.2.1. Acid Activation of Bentonite

The acid activation step of bentonite was performed to remove metallic and carbonate impurities. The activation processes were accomplished using 100 mL of diluted sulfuric acid (20%) in the presence of 10 g of raw bentonite. Homogenization between the bentonite fractions and acid was performed for 12 h at 100 °C using a magnetic stirrer at an adjustable speed of 650 rpm. The activated bentonite was then separated from the acid solution by filtration using whatman filter paper, neutralized by washing with distilled water, and dried at room temperature (40.3 °C) for 48 h. Subsequently, the sample was maintained for further characterization and synthesis.

2.2.2. Synthesis of Curcumin Intercalated Bentonite (CU/BE)

Curcumin-intercalated bentonite was prepared to support the main phytochemicals within the layered silicate host of bentonite. First, approximately 3.7 g of curcumin was dispersed in 100 mL of ethanol (60%) for 15 min using a magnetic stirrer at 1500 rpm and gentle temperature at 50 °C. This mixing step by the magnetic stirrer was followed by an additional homogenization step involving sonication of the curcumin/ethanol mixture for approximately 20 min at a power of 240 W. The obtained curcumin extract (50 mL) was added to a previously prepared colloid solution of bentonite fractions (4.4 g of bentonite in 50 mL of distilled water). The bentonite/curcumin extract mixture was homogenized for 12 h with stirring at 1500 rpm. The mixture was then transferred to a sonication bath for an additional 5 h to confirm the successful intercalation of the bentonite layers with the

phytochemicals of the curcumin extract. Finally, the obtained solid product was extracted from the residual solution, washed several times, and dried for 12 h at 50 °C (Figure 1).

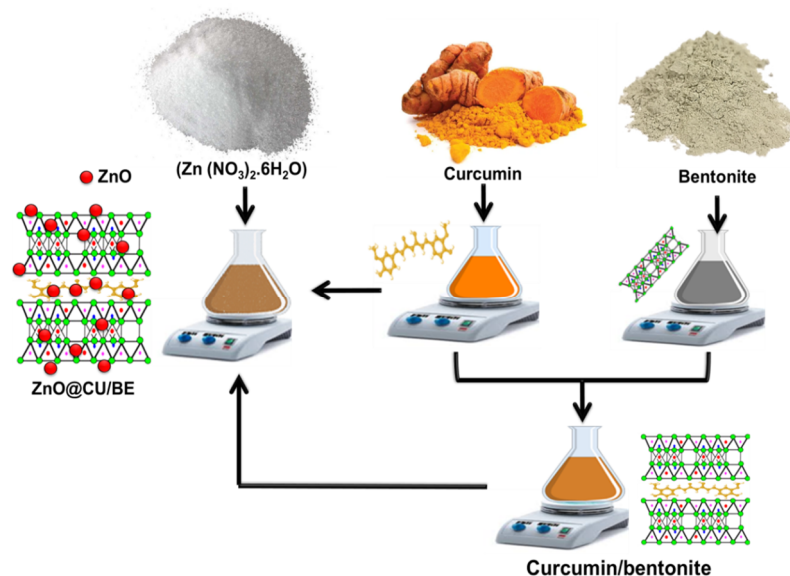


Figure 1. Schematic diagram for the synthesis procedures of curcumin intercalated bentonite (50 mL bentonite suspension ((4.4 g) + 50 mL water) + 50 mL curcumin extract (3.7 g of curcumin + 100 mL of ethanol (60%)) and ZnO@CU/BE composite (100 mL bentonite/zinc nitrate mixture (4.4 g bentonite + 2.2 g of $Zn(NO_3)_2 \cdot 6H_2O$) + 100 mL water) + 100 mL curcumin extract (3.7 g of curcumin + 100 mL of ethanol (60%))).

2.2.3. Synthesis of ZnO@ Benetonite Mediated Curcumin Extract (ZnO@CU/BE)

The green decoration of bentonite with ZnO nanoparticles involved the preparation of curcumin green extract as the applied reducing and capping reagent according to the procedures reported in Section 2.2.2. As a parallel step, 4.4 g of bentonite was dispersed within an aqueous solution of zinc nitrate (100 mL; 2.2 g of $Zn(NO_3)_2 \cdot 6H_2O$) with stirring for 10 h at 650 rpm. The solution was then subjected to sonication waves (250 W) for additional 2 h. The sonication step was followed by the addition of the curcumin extract (100 mL) to the prepared bentonite/zinc nitrate mixture with high-speed stirring until a dark red precipitate was detected. The stirring process was continued for 24 h at five intervals of 20 min of sonication to confirm the homogenous distribution of the formed zinc oxide or zinc oxide/curcumin complexes throughout the bentonite host. The product was extracted after this step by filtration, washed carefully with distilled water for several times, dried overnight at 50 °C, labeled as ZnO@CU/BE, and stored in glass containers at 25 °C for further characterization and testing (Figure 1).

2.3. Characterization Methods

The crystalline properties and structural effects of the compounds obtained after the modification steps were determined based on the X-ray diffraction patterns. The patterns were obtained using a PANalytical-Empyrean X-ray diffractometer with a measuring range of 5–80°. The functional chemical groups during the synthesis procedures were illustrated based on the FT-IR spectrum obtained using a Fourier-transform infrared spectrometer (FTIR–8400S; Shimadzu) with a measuring range of 400 cm^{-1} to 4000 cm^{-1} . The morphological changes in terms of different modification steps were examined based on SEM images obtained using a scanning electron microscope (Gemini, Zeiss-Ultra 55) and HRTEM images obtained using a transmission electron microscope (JEOL-JEM2100). The textural properties in terms of the specific surface area and porosity were described based on the N_2 adsorption/desorption isotherm curves determined using a surface area analyzer (Beckman Coulter SA3100).

2.4. Antioxidant Activities

2.4.1. Nitric Oxide Radical Scavenging Assay

The scavenging of nitric oxide by the prepared structures was assessed based on the procedure reported by Kitture et al. [40]. The prepared solutions of the synthetic structures (20 μL ; 100 $\mu\text{g}/\text{mL}$) were mixed with 2 mL of sodium nitroprusside (10 mM) in saline phosphate buffer solution (500 μL , pH 7.4). The mixed solutions were incubated for 150 min at 25 $^{\circ}\text{C}$. By the end of the incubation period, 500 μL of the obtained mixture is taken and mixed with sulfanilic acid (1 mL), which was prepared by diluting 33% of it with 20% glacial acetic acid before incubation again for an additional 5 min. Naphthyl ethylenediamine dihydrochloride (1 mL; 0.1% *w/v*) was then added to the incubated mixture, which was re-incubated again for 30 min. By the end of the incubation process, the scavenging percentages of nitric oxide were calculated according to Equation (1) after determining the absorbance at 540 nm.

$$\text{Scavenging (\%)} = \frac{A_{540\text{Control}} - A_{540\text{Test}}}{A_{540\text{Control}}} \times 100 \quad (1)$$

2.4.2. DPPH Radical Scavenging Assay

The efficiency of the synthetic structures as scavengers of DPPH radicals was assessed based on the method reported by Robkhob et al. [7]. The synthetic structures (20 μL ; 100 $\mu\text{g}/\text{mL}$) were mixed homogeneously in 96-well plates with methanolic solution (80 μL) composed of DPPH (100 μM). After the mixing step, the system was incubated in the dark for 20 min, and the changes in absorbance after the incubation period were determined using a microplate reader at an estimated wavelength of 517 nm. The measured values were used in the direct calculation of the scavenging percentages according to Equation (2).

$$\text{Scavenging (\%)} = \frac{A_{517\text{Control}} - A_{517\text{Test}}}{A_{517\text{Control}}} \times 100 \quad (2)$$

2.4.3. ABTS Radical Scavenging Assay

The scavenging properties of the prepared materials were evaluated based on the procedures presented by Dappula et al. [41]. A stock solution of ABTS (7 mM) was prepared by dissolving 44 mg of ABTS in 10 mL of deionized water, which was mixed with another solution of potassium persulfate (3 μL) to generate ABTS radicals ($\text{ABTS}^{\bullet+}$) by incubating the system for 18 h in the dark at 25 $^{\circ}\text{C}$. The generation of the $\text{ABTS}^{\bullet+}$ was followed by the addition of methanol at a ratio of 1:29 to obtain fresh $\text{ABTS}^{\bullet+}$. The prepared structures (10 μL ; 100 $\mu\text{g}/\text{mL}$) were then mixed with the ABTS solution (290 μL) for 30 min. By determining the absorbance of the solutions in the absence (control) and presence of the structure (test) at 734 nm, the scavenging percentages of the ABTS radicals were calculated according to Equation (3).

$$\text{Scavenging (\%)} = \frac{A_{734\text{Control}} - A_{734\text{Test}}}{A_{734\text{Control}}} \times 100 \quad (3)$$

2.4.4. Superoxide Radical Scavenging Assay

The scavenging efficiency of superoxide radicals released by the synthetic structures was assessed according to the procedure reported by Robkhob et al. [7]. The scavenging process involved mixing the prepared structures (100 μL ; 100 $\mu\text{g}/\text{mL}$) with a riboflavin solution (100 μL ; 20 μg), EDTA solution (200 μL ; 12 mM), ethanol (0.1 mM; 200 μL), and NBT (100 μL ; 0.1 mg). The obtained mixture was diluted with phosphate buffer (3 mL, 50 mM) and exposed to an illumination source for 5 min. By determining the absorbance of the solu-

tions in the absence (control) and presence of the structure (test) at 540 nm, the scavenging percentages of the superoxide radicals were calculated according to Equation (4).

$$\text{Scavenging (\%)} = \frac{A540_{\text{Control}} - A540_{\text{Test}}}{A540_{\text{Control}}} \times 100 \quad (4)$$

2.5. Antidiabetic Studies

2.5.1. Porcine Pancreatic α -Amylase Inhibition Assay

The antidiabetic properties of the synthetic structure were assessed based on the α -amylase inhibition assay using the previously reported chromogenic 3,5-dinitrosalicylic acid (DNSA) method [7]. The synthetic products (500 μ L; 100 μ g/mL) were incubated with porcine pancreatic α -amylase (100 μ L; 50 μ g/mL) for 10 min at 37 °C and followed by the careful addition of starch substrate (1.5 mL; 1%). The absorbance of α -amylase in the presence (test) and absence (control) of the synthetic products was measured at 540 nm, and the obtained results were used to calculate their inhabitation percentage according to Equation (5).

$$\text{Inhibition (\%)} = \frac{A540_{\text{Control}} - A540_{\text{Test}}}{A540_{\text{Control}}} \times 100 \quad (5)$$

2.5.2. Crude Murine Pancreatic α -Amylase Inhibition Assay

The effect of the synthetic products on the enzymes of the crude murine model was assessed to confirm their potential as antidiabetic agents. The pancreas of a Swiss male mouse (ten-week-old) was used as the source of the studied enzymes, which was subjected to starvation for 12 h. Subsequently, it was homogenized and excised in saline phosphate buffer supplemented with protease inhibitors. This was followed by centrifugation at 10,000 rpm for 15 min to isolate cell-free supernatant. The isolated cells were diluted to obtain an absorbance of 0.4 at 280 nm and used as the tested source of crude enzyme. Crude murine pancreatic amylase was inhibited according to the steps described in Section 2.5.1.

2.5.3. α -Glucosidase Inhibition Assay

The inhibitory effect of the synthetic products on α -glucosidase was investigated according to the methodology reported by Sanap et al. [42]. The synthetic products (200 μ L; 100 μ g/mL) were mixed with 100 μ L of the tested α -glucosidase (100 μ L; 0.1 unit/mL), followed by incubation for 60 min at 37 °C. Then, 10 μ L of p-nitrophenyl- α -D-glucopyranoside (pNPG) was added to the incubated mixture, which was incubated again for an additional 10 min at the same temperature. Subsequently, 2 mL of Na₂CO₃ (0.1 M) was added to the system to stop the reaction. The absorbance of nitrophenol diffused from pNPG was determined using a microplate reader at a wavelength of 420 nm, and the values were used to estimate the inhibition percentages according to Equation (6).

$$\text{Inhibition (\%)} = \frac{A420_{\text{Control}} - A420_{\text{Test}}}{A420_{\text{Control}}} \times 100 \quad (6)$$

2.5.4. Crude Murine Intestinal α -Glucosidase Inhibition Assay

Swiss male mice were used as the source of crude intestinal α -glucosidase used during the test, considering the preparation procedures reported in the Section 2.5.2. Moreover, the inhibitory potential of the prepared products on crude murine intestinal α -glucosidase was studied according to the steps reported in Section 2.5.3 in the presence of a p-nitrophenyl- α -D-glucopyranoside substrate.

2.5.5. Amyloglucosidase Inhibition Assay

The inhibitory properties of the synthetic structures against amyloglucosidase were estimated according to Lawande et al. [43]. The prepared materials (100 μ L; 100 μ g/mL) were mixed with amyloglucosidase (100 μ L; 0.1 unit/mL) and incubated at 37 °C for 10 min in the presence of starch substrate (1%). The absorbance of amyloglucosidase in the

presence (test) and absence (control) of the synthetic products was measured at 540 nm, and the obtained results were used to calculate their inhabitation percentages according to Equation (5).

2.6. Statistical Analysis

The presented values in the study represent the mean values \pm the standard error of the mean (S.E.M.; $n = 3$), and the significance of the statistical evaluation was assessed based on the analysis results of variance (ANOVA) as well as paired tests considering the value of $*p < 0.05$.

3. Result and Discussion

3.1. Characterization of the Synthetic Structure

3.1.1. Structural Properties

The crystalline and structural properties of raw bentonite, activated samples, and synthetic ZnO@CU/BE were assessed based on their XRD patterns. The resultant pattern of the raw sample shows the common diffraction peaks of bentonite. Montmorillonite was identified as the dominant and essential phase of clay minerals with peaks at 5.78° (001) and 6.95° (002), in addition to other peaks at 19.85° , 21.54° , 26.68° , and 28.56° (Ref. card No: 000-003-0010) (Figure 2 (A)). In addition, the recognized pattern demonstrated the existence of clay (kaolinite) and non-clay (quartz) impurities, which are common in natural bentonite (Figure 2 (A)). The detected montmorillonite phase exhibited an average crystallite size of 12.9 nm and basal spacing of 12.71 Å. After the acid activation step, the resulting pattern demonstrated the apparent effects of sulfuric acid on the sample and structure of the montmorillonite phase (Figure 2 (B)). A remarkable decline was noted in the previously identified peaks of montmorillonite as well as a deviation in the position of the main peaks to lower angles ($2\theta = 5.05^\circ$ and 6.6°), which has been documented widely in acid-activated bentonite (Figure 2 (B)) [44–46]. Such changes in the XRD diffraction peaks validate the partial deformation impacts of the acid activation steps on the structure of bentonite, which might be associated with an enhancement in the surface reactivity and textural properties.

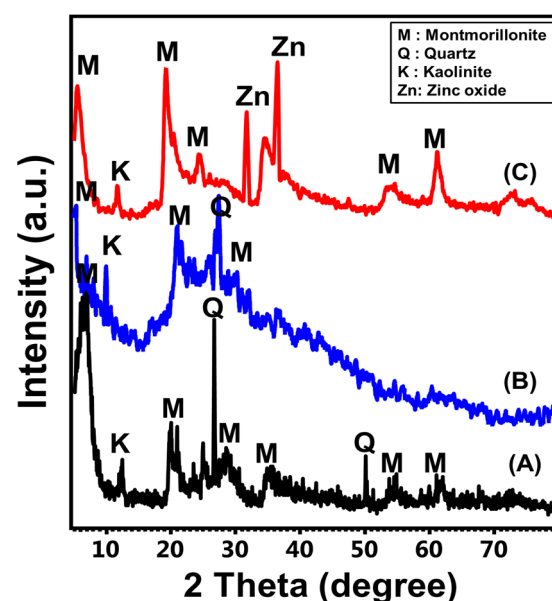


Figure 2. XRD patterns of raw bentonite (A), acid activated bentonite (B), the synthetic ZnO@CU/BE structure (C).

Regarding the obtained pattern of the prepared ZnO@CU/BE, the recognized peaks revealed significant changes in the structure of bentonite as well as the identification of different crystalline phases (Figure 2 (C)). First, the obtained pattern reflected significant

enhancement in intensifying some of the common montmorillonite peaks but at deviated positions (6.48° , 20.12° , and 25.35°) as well as the basal spacing value (13.61 \AA) (Figure 2 (C)). The deviation in the positions of the peaks and the increment in the basal spacing validate the significant effect of successfully intercalated curcumin-related phytochemicals between the montmorillonite layers. The absence of peaks related to the curcumin structure suggested molecular-level dispersion as well as disordered crystalline properties of its structure as intercalated organic components within the montmorillonite layers [47]. Moreover, new peaks were detected at sharp intensities, signifying significant decoration of the curcumin/bentonite structure with green ZnO nanoparticles of the wurtzite structure (Figure 2 (C)). Good diffraction peaks of ZnO were observed at 31.65° (100) and 36.4° (101), in addition to other peaks that might overlap with some montmorillonite peaks, especially around 34° and 56° (Figure 2 (C)) (JCPDS no. 79-2205; JCPDS no. 65-3411).

3.1.2. Morphological and Textural Properties

The morphological features were significantly affected by the different modification and hybridization processes. The changes in the surface, as well as the internal features of bentonite during the different functionalization steps, were observed based on the SEM and HRTEM images (Figure 3). The raw bentonite appeared in the SEM images as aggregated clusters of compacted and stacked flake grains, which are common features of clay minerals. The high-magnification SEM images revealed the characteristic cornflake morphology of the montmorillonite grains with observable flexing and curvature of their platelets, forming notable lenticular secondary pores (Figure 3A). The studied HRTEM images of BE particles reflected their common internal structure, as they exhibited observable multilayered properties with a known lattice structure, which is a characteristic feature of the montmorillonite phyllosilicate structure (Figure 3B). The intercalation of the bentonite sheets with the extracted phytochemicals of curcumin exhibited considerable exfoliation effects, as the structural clay layers appeared to be displaced from each other in the SEM images (Figure 3C). The bentonite fractions appeared as swollen particles compared with the reported compacted aggregates of the raw sample (Figure 3C). This is in agreement with the results of HRTEM, as the bentonite grains appeared to be hybridized by polymeric films of nearly fibrous forms and rendered a darker gray tone to the grains than that of the commonly detected bentonite grains (Figure 3D). After the green decoration step of curcumin intercalated bentonite (CU/BE) particles with the ZnO nanoparticles, the SEM images reflected the remarkable distribution of the formed ZnO nanoparticles on their surfaces with irregular to spherical forms (Figure 3E). This was also confirmed by HRTEM images, which indicated the presence of metal oxide nanoparticles (ZnO) as inclusions between the intercalated bentonite layers and its surface (Figure 3F).

Previously reported morphological changes were associated with significant textural changes in terms of surface area and porosity properties. The surface area was enhanced notably from $91 \text{ m}^2/\text{g}$ for raw bentonite (BE) to $98.7 \text{ m}^2/\text{g}$, $106.3 \text{ m}^2/\text{g}$, and $118.4 \text{ m}^2/\text{g}$ for the prepared acid-activated BE, CU/BE, and ZnO@CU/BE, respectively. The enhancement in the surface area signifies the impact of the acid activation step on the surface area, as well as the effect of the intercalation process of the bentonite layers with extracts of curcumin in expanding the basal spacing, which is associated with an enhancement in the surface area. In addition, the presence of ZnO as decorated nanograins on the surface of the structure imparted an irregular typography to the surface, which induces surface area.

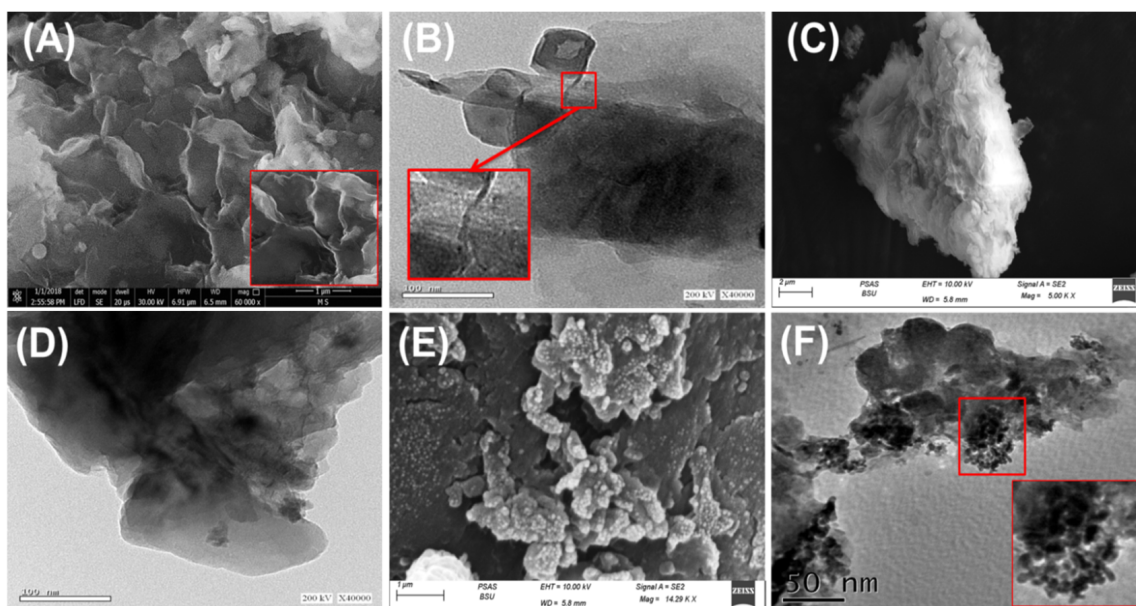


Figure 3. SEM image of raw bentonite (A) [48], HRTEM image of raw bentonite (B) [49], SEM images of synthetic CU/BE composite (C), HRTEM image of the synthetic CU/BE composite (D), SEM image of the synthetic ZnO@CU/BE composite (E), and HRTEM image of the synthetic ZnO@CU/BE composite (F).

3.1.3. Chemical Properties

The modification effects on the chemical properties of the obtained structures as well as the dominant chemical groups were determined based on the FT-IR spectra of the prepared materials (Figure 4). The spectrum of the bentonite precursor clearly displayed the essential bands of structural -OH groups (3400 cm^{-1}) that coordinate to the octahedral cations (Al_2OH , $\text{AlMg}(\text{OH})$, and $\text{AlFe}^{3+}(\text{OH})$) and the characteristic interlayer molecules of the montmorillonite structure (1640 cm^{-1}) (Figure 4 (A)). Moreover, the Si-O and Al-O groups were clearly signified by the observed bands at approximately 1000 cm^{-1} and 918 cm^{-1} , respectively. The recognized bands within the determination area from 400 cm^{-1} to 1000 cm^{-1} corresponded to the bending vibrations of Si-O-Al (520 cm^{-1}), Si-O-Si (466 cm^{-1}), Si-O-Mg, and Mg-Fe-OH (Figure 4 (A)) [49,50]. The spectrum of bentonite after the acid activation step demonstrated no remarkable changes in the identification bands of the bentonite chemical structure, except for the observable deviation in the positions of the bands, as well as the strong intensification in the absorption bands of structural hydroxyl groups and interlayered water molecules (Figure 4 (B)). This finding reflects the significant hydration effects of the acid treatment processes and demonstrates the non-extensive destruction effect of the acid activation reactions of the structural units of montmorillonite.

Regarding the FT-IR spectrum of curcumin as separated components, the observable bands identified the hydroxyl groups of the phenolic phytochemicals (3506 cm^{-1}), aromatic C-H of neat curcumin (2943 and 2965 cm^{-1}), stretching vibration of C=C (1626.3 cm^{-1}), aromatic benzene rings of curcumin (1604.2 cm^{-1}), the vibration of C=O (1507 cm^{-1}), olefin C-H (1432 cm^{-1}), aromatic C-O (1278.6 cm^{-1}), aromatic C-H (1162 and 812 cm^{-1}), C-O-C (1023 cm^{-1}), benzoatetrans-CH (963 cm^{-1}), and aromatic cis-CH (716 cm^{-1}) (Figure 4 (C)) [30,37,47]. Upon comparing the spectrum of the CU/BE hybridized product with both separated bentonite and curcumin spectra, the resultant spectrum demonstrated complex related organic/inorganic chemical groups but with considerable deviation in their identification absorption bands (Figure 4 (D)). This signified the successful and effective intercalation of bentonite sheets with the phytochemical compounds extracted from curcumin. While Si-O (1008 cm^{-1}), Al-O (934 cm^{-1}), Si-O-Al (534 cm^{-1}), and Si-O-Si (473.2 cm^{-1}) were detected clearly as characteristic groups of bentonite, the curcumin phytochemicals were identified signif-

icantly by benzene rings (1612 cm^{-1}), C=O (1509 cm^{-1}), olefin C-H (1440 cm^{-1}), aromatic C-O (1284 cm^{-1}), and benzoatetrans-CH (921 cm^{-1}) (Figure 4 (D)). The same complex organic/inorganic functional groups were also identified in the FT-IR spectrum of ZnO@CU/BE but at shifted positions because of the interaction effects of the decorated ZnO nanoparticles (Figure 4 (E)). Moreover, the stretching vibration of the Zn-O bond was clearly detected by the notable absorption band at 620 cm^{-1} [28,29].

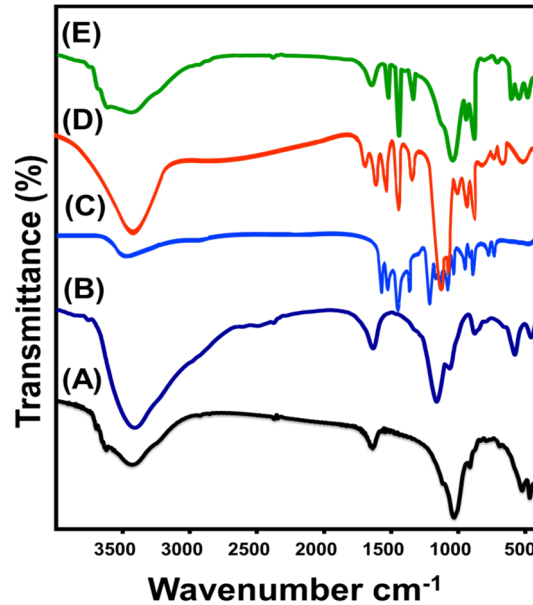


Figure 4. FT-IR spectrum of raw bentonite (A), acid activated bentonite bentonite (B), curcumin powder (C), synthetic CU/BE composite (D), and synthetic ZnO@CU/BE composite (E).

The previously reported FT-IR findings on the intercalation of bentonite sheets with curcumin-based phytochemicals, as well as the successful decoration of the structure with ZnO, are in agreement with the elemental EDX analysis (Figure 5). The EDX spectrum of the composite (ZnO@CU/BE) demonstrated the presence of the characteristic elements of bentonite (Si and Al), curcumin extract (C), and ZnO (Zn), in addition to the significant oxygen content, which reflected the impact of the intercalated organic phytochemical extracts of curcumin (Figure 5).

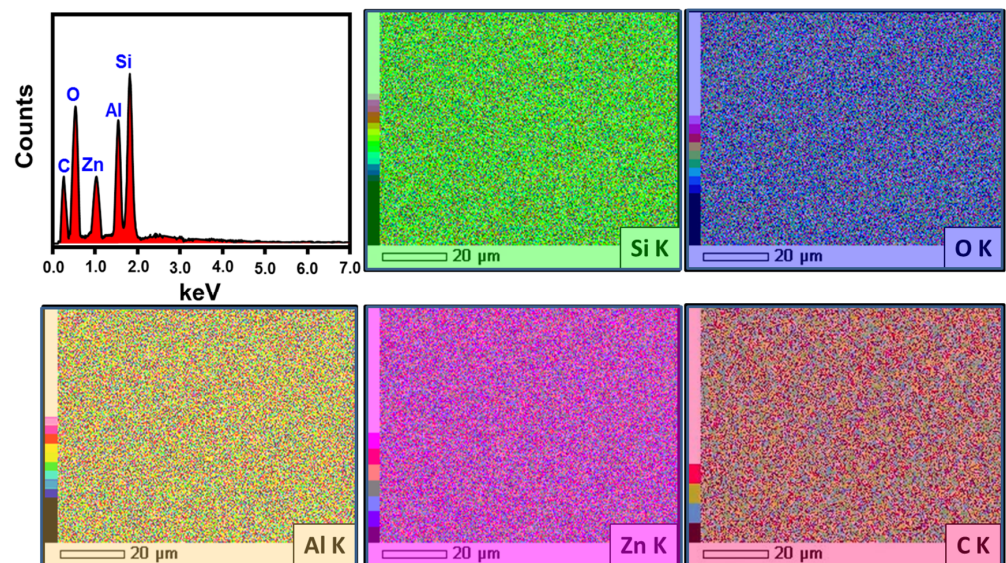


Figure 5. EDX spectrum and mapping of the synthetic ZnO@CU/BE composite.

3.2. Antioxidant Properties

3.2.1. Nitric Oxide Scavenging

Typically, common reactive oxygen species (ROS) are by-products of aerobic respiration and electron transportation. The release of these active radicals results in considerable oxidative stress, which is represented by a controlled increase in intracellular ROS levels and causes several degenerative diseases [51]. Moreover, the presence of nitric oxide free radicals at higher levels may induce damage to cells along with cytotoxic effects on cells, neuronal cell death, and DNA fragmentation [52]. Metals, as well as metal oxide-based materials, especially in their nanoforms, exhibit promising antioxidant properties and are used at effective rates against nitric oxide radicals. The nitric oxide active radicals are gaseous free radicals that exhibit damaging and beneficial biological effects [7,53]. The scavenging and trapping efficiencies of nitric oxide radicals by CU, CU/BE, green ZnO, and ZnO@CU/BE demonstrated the significant potential of the ZnO@CU/BE composite ($88.6 \pm 1.58\%$) as compared to that of CU ($12.3 \pm 1.06\%$), CU/BE ($23.6 \pm 1.17\%$), and green ZnO ($48.7 \pm 1.36\%$) as well as the ascorbic acid standard ($21.6 \pm 1.33\%$) (Figure 6A). These results validate the preference for applying the composite as a recommended drug candidate compared to the curcumin extract or ZnO, as it demonstrated the best nitric oxide scavenging capacity in addition to the significant biocompatible properties of bentonite. This remarkable enhancement effect of the bentonite host as the carrier might be attributed to the excellent adsorption and absorption capacities of bentonite, leading to the induction of the capture and trapping of nitric oxide. Moreover, it enhanced the stability, dispersion, and exposure of the interactive interfaces between the loaded bioactive compounds (ZnO and curcumin-based phytochemicals) and nitric oxide radicals [24,54]. Finally, the developed composite introduced novel structures of multifunctional active groups with antioxidant affinities towards free nitric oxide active radicals. Moreover, the encapsulation of curcumin extract within the bentonite layers enhanced its antioxidant activity by promoting its solubility compared to the limited solubility of pure curcumin [55].

3.2.2. DPPH Radical Scavenging

The DPPH radical scavenging properties of CU, CU/BE, green ZnO, and ZnO@CU/BE were studied using synergetic procedures. The determined results demonstrated the significant scavenging efficiency of DPPH radicals by the synthetic ZnO@CU/BE composite ($90.2 \pm 1.76\%$) compared to that of CU ($62.5 \pm 1.62\%$), CU/BE ($74.8 \pm 1.41\%$), and green ZnO ($56.3 \pm 1.37\%$) as well as the ascorbic acid standard ($76.3 \pm 1.28\%$) (Figure 6B). Moreover, the obtained activity by the composite is significantly higher than several investigated structures in the literature such as Ag doped ZnO (73.79%) [7], CuO (about 80%) [56], Ag nanoparticles (67%) [57], RGO-ZnO NCs (69%) [15], Pt nanoparticles (70%) [58], and Au nanoparticles (70.73%) [59]. Generally, the DPPH scavenging mechanism of the prepared ZnO@CU/BE composite involves the significant transfer of an electron (e^-) and proton (H^+) to the organic DPPH radical, suggesting coupled proton/electron transfer reactions [5]. The essential antioxidant mechanism is mediated by the loaded ZnO and involves the transmission of the electron density, which is positioned at oxygen, to the common odd electron that is situated at the nitrogen atom within the structure of DPPH [41]. The bentonite carrier exhibited strong inducing effects on a previously reported mechanism. The negatively charged surface of the bentonite layers might enhance the charge separation efficiency via electron attraction processes, which, in turn, enhances the antioxidation activity of the final composite (ZnO@CU/BE) [60].

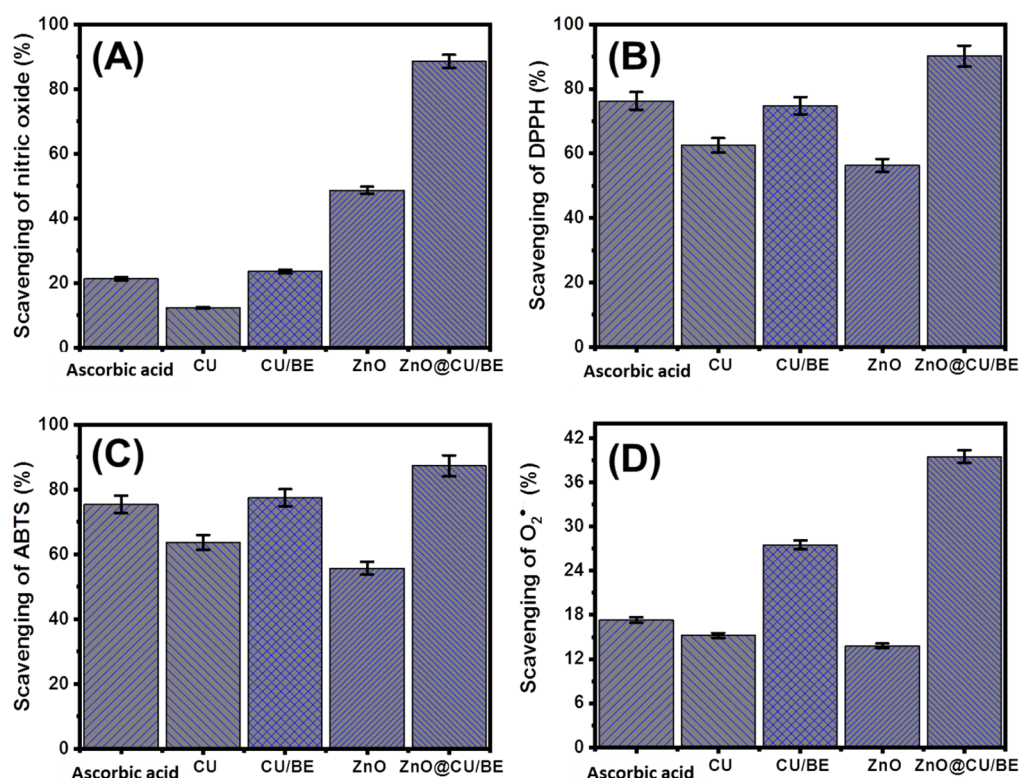


Figure 6. The antioxidant activities of CU, CU/BE, green ZnO, and ZnO@CU/BE structures (100 $\mu\text{g}/\text{mL}$) as compared to ascorbic acid as positive control; (A) nitric oxide scavenging activities (20 μL ; 100 $\mu\text{g}/\text{mL}$); (B) DPPH scavenging activities (20 μL ; 100 $\mu\text{g}/\text{mL}$); (C) ABTS scavenging activities (10 μL ; 100 $\mu\text{g}/\text{mL}$); and (D) super oxide radical scavenging activities (100 μL ; 100 $\mu\text{g}/\text{mL}$).

3.2.3. ABTS Radical Scavenging

The ABTS scavenging test has recently been recommended to evaluate the antioxidant properties of different compounds, especially complex structures and hybrid materials. This assay involves the generation of ABTS cation radical ($\text{ABTS}^{\cdot+}$) using potassium persulfate. Therefore, the synthetic structures that exhibit hydrogen-donating antioxidant properties, as detected in the synthetic ZnO@CU/BE (ZnO and curcumin), will be very effective in reducing the released $\text{ABTS}^{\cdot+}$. The scavenging properties of CU, CU/BE, green ZnO, and ZnO@CU/BE against the ABTS radical were studied using synergetic procedures, with ascorbic acid as a control (Figure 6C). The determined results are in agreement with previously reported scavenging results for other radicals. These results reflected the higher activity of the synthetic ZnO@CU/BE composite ($87.3 \pm 1.61\%$) than that of CU ($63.7 \pm 1.35\%$), CU/BE ($77.4 \pm 1.83\%$), green ZnO ($55.7 \pm 1.44\%$), and ascorbic acid standard ($75.4 \pm 1.14\%$) (Figure 6C). The recognized ABTS scavenging activity by the composite is higher than the reported activity using several investigated materials such as oregano oil/halloysite [61], mung bean protein [62], soy β -conglycinin-dextran-polyphenol [55], and chitosan/lignosulfonate micelles [63]. In addition to the previously reported enhancement effects of the bentonite carrier on the physicochemical properties of the loaded green ZnO, the wrapping of curcumin-based phytochemicals between the bentonite layers effectively contributed to the generation of hydrogen atoms [24].

3.2.4. Superoxide Radical Scavenging

Active superoxide anion radicals ($O_2^{\bullet-}$) are produced mainly by cellular organelles, such as mitochondria, and are immediately transformed into active hydroxyl radicals ($\bullet OH$) and hydrogen peroxide (H_2O_2). The human body exhibits a natural defense system against superoxide radicals and other reactive radicals to maintain effective physiological homeostasis; however, sometimes nonfunctional or noneffective values are also observed, as has been widely detected in various diseases. The uncontrolled release of active oxygenated radicals and the nonregulation of their levels are associated with severe pathophysiological conditions and, in turn, degenerative diseases that pose significant health risks [64]. The determined results demonstrate strong scavenging percentages of $O_2^{\bullet-}$ associated with the synthetic ZnO@CU/BE composite ($39.5 \pm 1.12\%$) as compared to those related to CU ($15.2 \pm 1.66\%$), CU/BE ($27.5 \pm 1.31\%$), and green ZnO ($13.8 \pm 1.22\%$) as well as the ascorbic acid standard ($17.3 \pm 1.34\%$) (Figure 6D). Moreover, the obtained activity by the composite is significantly higher than several investigated structures in the literature such as Ag doped ZnO (27.34%) [7], CuO (about 80%) [56], and Ag nanoparticles [57]. Therefore, the prepared ZnO@CU/BE green structures can be deemed promising scavenging or trapping agents for superoxide radicals. This provides protection against cellular damage as it can strongly hinder the interaction between superoxide species and cellular molecules, including RNA, DNA, and proteins [65].

3.3. Antidiabetic Properties

3.3.1. Porcine Pancreatic α -Amylase Inhibition Assay

The inhibitory effects of the commonly used antidiabetic structures on α -amylase were examined. The results exhibited significant preventive effects on the breakdown reactions of complex sugars into simple chemicals, which strongly hinders the absorption efficiency of dietary starches and, in turn, controls postprandial hyperglycemia in diabetes [28]. The α -amylase inhibitory activities of CU, CU/BE, green ZnO, and ZnO@CU/BE were determined in synergetic studies and are presented in Figure 6A. The inhibitory properties of the CU extract, CU/BE, green ZnO, and ZnO@CU/BE prepared structures against porcine pancreatic α -amylase were significantly enhanced at different stages of the hybridization process (Figure 7A). The determined inhibition percentages of CU extract and CU/BE were $54.3 \pm 1.46\%$ and $60.7 \pm 1.77\%$, respectively (Figure 7A). An enhancement of approximately 6.4% was observed after the intercalation of curcumin extracts within the layered structure of montmorillonite, which might be attributed to the role of the montmorillonite host in controlling the release rate of loaded active phytochemicals and, in turn, preserving their impact on the enzyme for long intervals. The determined inhibition percentage of green ZnO was $44.5 \pm 1.53\%$ which was significantly lower than the determined value of ZnO@CU/BE ($76.8 \pm 1.87\%$). This value was higher than the values of CU extract and CU/BE as well as those of the assessed standards of the commercially used drugs (miglitol ($18.3 \pm 1.42\%$) and acarbose ($75.2 \pm 1.68\%$)) (Figure 7A). This might be attributed to the significantly high surface area of the bentonite layers, which enhanced the dispersion, stability, and exposure properties of the supported green ZnO nanoparticles and prevented adverse agglomeration, thereby, increasing the interaction area or interface with the enzyme. The aggregation and agglomeration of synthetic nanoparticles lead to the degeneration of their biological activities [24]. This is in agreement with the results of previous studies examining the impact of carriers on enhancing the antidiabetic and biological activities of curcumin and ZnO [15,24,30,66]. The recognized activity of ZnO@CU/BE is significantly higher than several studied structures in the literature such as Ag doped ZnO (23%) [7], Ag/CuO (38.9%) [67], RGO-ZnO (51.19%) [15], Ag nanoparticle (61%) [57], NiO nanoparticles (22%) [67], and synthetic Fe-CuO-SiO₂ composite [68].

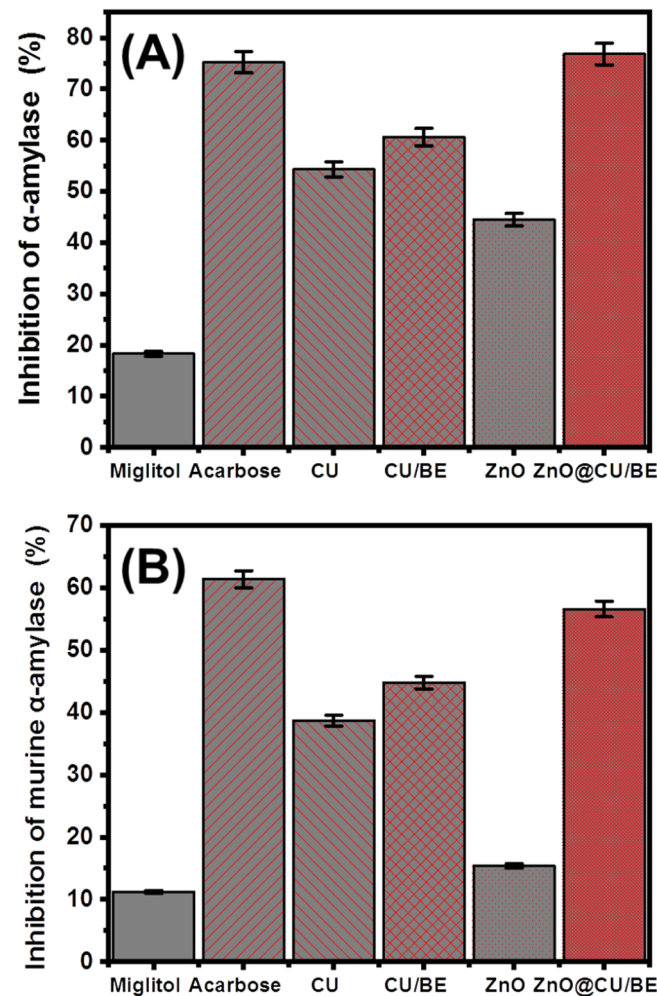


Figure 7. The α -amylase inhibition activities of CU, CU/BE, green ZnO, and ZnO@CU/BE structures as compared to the positive control miglitol and acarbose (500 μ L; 100 μ g/mL); (A) porcine pancreatic α -amylase enzyme (100 μ L; 50 μ g/mL); and (B) murine pancreatic α -amylase enzyme (100 μ L; 50 μ g/mL).

The α -amylases are effective and dominant digestive enzymes that exhibit a strong capacity to break down the long-chain polymeric structure of carbohydrates, such as polysaccharide starch into smaller structures of maltose, which are immediately transformed into glucose forms [7]. Therefore, their effective inhibition significantly reduces blood sugar levels [69]. The results obtained using CU/BE, green ZnO, and ZnO@CU/BE validate their significant potential for use as antidiabetic agents, considering the reported value of the commonly used drugs miglitol and acarbose. Some of the commercially used enzyme inhibitors, such as acarbose, exhibit significantly high inhibition values at the highest concentrations. However, they are still expensive compared to natural products, in addition to the commonly demonstrated side effects with their applications [70,71].

3.3.2. Murine Pancreatic α -Amylase Inhibition

The inhibitory potential of CU extract, CU/BE, green ZnO, and ZnO@CU/BE structures was evaluated against crude murine pancreatic α -amylase. However, the recognized results demonstrate lower inhibition effects than the reported results against porcine pancreatic α -amylase; the results signify the enhancement in the inhibition activity with the different hybridization processes. The application of CU extract and CU/BE resulted in inhibition percentages of $38.7 \pm 1.33\%$ and $44.8 \pm 1.52\%$, respectively, with notable enhancement by approximately 6% (Figure 7B). The application of ZnO@CU/BE showed an inhibition percentage of $56.5 \pm 1.67\%$, which was higher than the determined value of green ZnO ($15.4 \pm 1.11\%$) by approximately 41%, compared to that of CU which was 17.8% and that of CU/BE which was 11.7% (Figure 7B). These results validate the significant inhibition properties of the synthetic ZnO@CU/BE composite against both the tested commercially available enzymes and the metabolically crude active enzymes considering the determined results using the controls miglitol ($11.2 \pm 1.61\%$) and acarbose ($61.4 \pm 1.55\%$) (Figure 7B).

3.3.3. Pancreatic α -Glucosidase Inhibition

Pancreatic and intestinal glycosidases are the most effective enzymes for the metabolism of dietary carbohydrates. Therefore, their inhibition demonstrates strong retarding effects on the absorption of glucose and, in turn, induces the suppression of hyperglycemia. The inhibitory properties of CU extract, CU/BE, green ZnO, and ZnO@CU/BE against α -glucosidase were determined and compared with those of commercially used miglitol and acarbose drugs, which were used as controls (Figure 8A). The determined percentages of inhibition against the assessed α -glucosidase enzyme corresponding to CU extract, CU/BE, green ZnO, and ZnO@CU/BE were $75.6 \pm 1.37\%$, $83.5 \pm 1.48\%$, $77.3 \pm 1.27\%$, and $96.5 \pm 1.07\%$, respectively (Figure 8A). This remarkable enhancement in the inhibition properties indicated the significant effect of the bentonite carrier in ensuring the stability, dispersal properties, exposure, and interactive interface of the effectively loaded functional groups of ZnO, as well as the extracted phytochemical curcumin. Moreover, the green fabrication of ZnO using the curcumin extract itself might result in the formation of curcumin/ZnO complexes or ZnO-capped curcumin structures that might exhibit potent inhibition properties, based on the previous literature [17]. The recognized activity of ZnO@CU/BE against α -glucosidase is significantly higher than several studied structures in the literature such as Ag doped ZnO (91.19%) [7], Ag/CuO (19.6%), and RGO-ZnO (53.24%) [15].

3.3.4. Murine Intestinal α -Glucosidase Inhibition

The synthetic products were also assessed as potential inhibitors of murine intestinal glucosidase. The synthetic hybridized products (CU/BE and ZnO@CU/BE) showed notable enhancement in the percentage inhibition against the evaluated murine intestinal glucosidase enzyme compared to the separated phases of curcumin extract and the green-fabricated ZnO based on the phytochemicals of the curcumin extract. The determined percentages of inhibition of the CU extract, CU/BE, green ZnO, and ZnO@CU/BE were $68.4 \pm 1.27\%$, $72.8 \pm 1.51\%$, $71.3 \pm 1.16\%$, and $92.5 \pm 1.10\%$, respectively (Figure 8B). Previous studies have reported a reduction in blood glucose levels using ZnO-based materials as antidiabetic agents, in addition to its effect of increasing the serum insulin, insulin receptor, glucokinase activity, and glucokinase genes [72]. Therefore, the present study demonstrated the development of a highly effective multifunctional antidiabetic structure (ZnO@CU/BE) at a low fabrication cost using simple and green methods based on natural resources and plant extracts.

3.3.5. Amyloglucosidase Inhibition

The properties of the synthetic ZnO@CU/BE structure as an antidiabetic agent in comparison with its integrated components were also based on their inhibitory effects on amyloglucosidase. The reported results also demonstrated significant inhibition of

the enzyme, with a remarkable augmentation in the inhibitory effects in the presence of the hybridized products (CU/BE and ZnO@CU/BE) rather than the separated phases of curcumin extract and the synthetic green ZnO nanoparticles (Figure 9). The observed percentages of inhibition of CU extract, CU/BE, green ZnO, and ZnO@CU/BE against amyloglucosidase enzyme were $65.8 \pm 1.35\%$, $83.4 \pm 1.47\%$, $70.5 \pm 1.77\%$, and $93.7 \pm 1.55\%$, respectively which are promising values considering the estimated inhibition percentages of the commercial drug used as controls (miglitol ($88.3 \pm 1.83\%$) and acarbose ($95.6 \pm 1.72\%$)) (Figure 9). Considering the previous results in comparison with the drug standards, the synthetic ZnO@CU/BE green composite can be used as a starch blocker with significant efficiency and can be applied to prevent the absorption of dietary starches by the human body owing to its inhibitory effects on the conversion of the complex sugar species into simple forms [72].

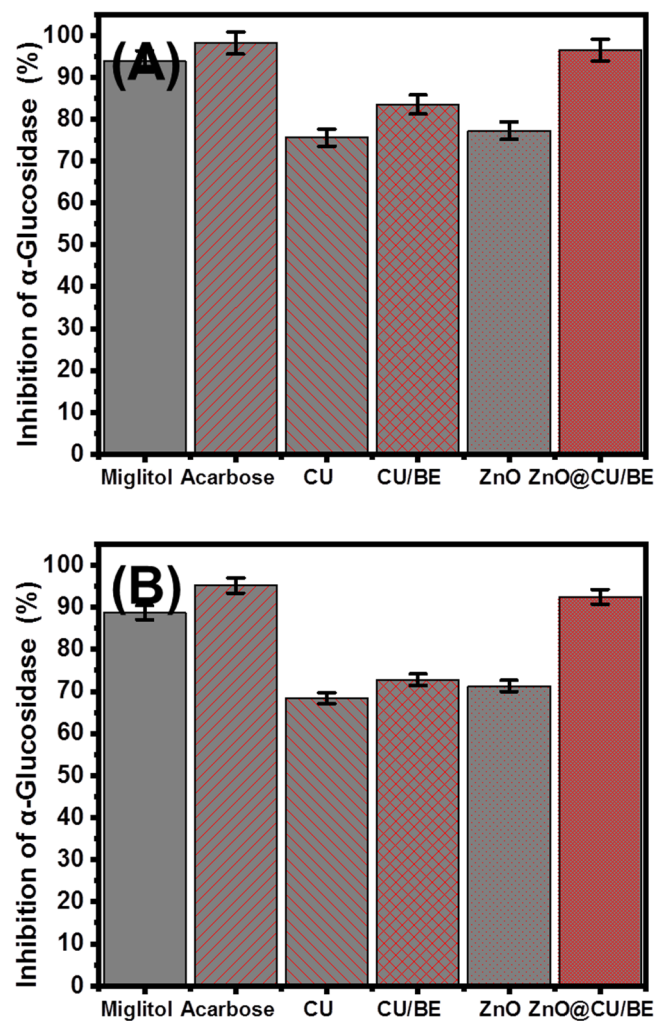


Figure 8. The α -glucosidase inhibition activities of CU, CU/BE, green ZnO, and ZnO@CU/BE structures as compared to the positive control miglitol and acarbose (200 μ L; 100 μ g/mL); (A) pancreatic α -glucosidase enzyme (100 μ L; 0.1 unit/mL); and (B) murine intestinal α -glucosidase enzyme (100 μ L; 0.1 unit/mL).

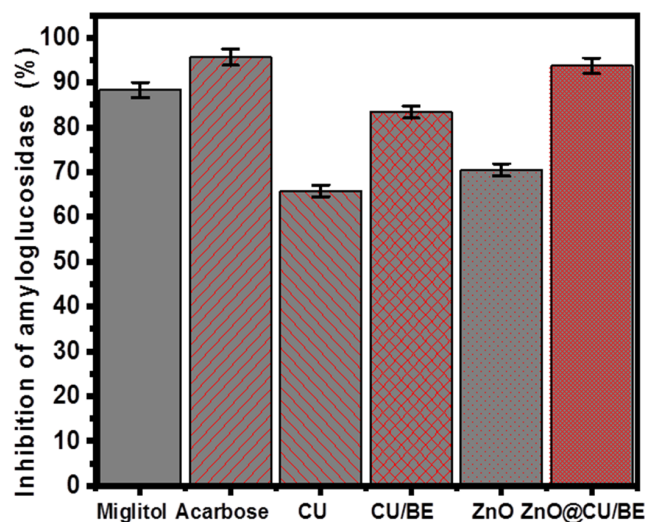


Figure 9. The amyloglucosidase (100 μ L; 0.1 unit/mL) inhibition activities of CU, CU/BE, green ZnO, and ZnO@CU/BE structures as compared to the positive control miglitol and acarbose (100 μ L; 100 μ g/mL).

4. Conclusions

A green ZnO-decorated acid-activated bentonite-mediated curcumin extract (ZnO@CU/BE) composite was synthesized via a facile green method using curcumin extract as an enhanced antioxidant and antidiabetic agent with multifunctional properties (curcumin-based phytochemicals, zinc oxide-capped curcumin, and zinc/curcumin complexes). It shows enhanced antioxidant and antidiabetic activities against the commonly studied radicals [nitric oxide ($88.6 \pm 1.58\%$), DPPH ($90.2 \pm 1.76\%$), ABTS ($87.3 \pm 1.61\%$), superoxide ($39.5 \pm 1.12\%$)] and enzymes [porcine pancreatic α -amylase ($76.8 \pm 1.87\%$), murine pancreatic α -amylase ($56.5 \pm 1.67\%$), pancreatic α -Glucosidase ($96.5 \pm 1.07\%$), murine intestinal α -Glucosidase ($92.5 \pm 1.10\%$), and amyloglucosidase ($93.7 \pm 1.55\%$)] compared to the commercial drugs and the separated components of the ZnO@CU/BE composite. The findings reflect the enhancement effect of bentonite carriers on the biological activities of curcumin-based phytochemicals and green ZnO. Therefore, the synthetic green ZnO@CU/BE composite can be recommended as enhanced, low-cost, biocompatible, safe, and simply produced antioxidant and antidiabetic agents compared to the commercially used drugs which will be covered by future in vivo studies.

Abbreviation

ZnO	Zinc oxide
CU	Curcumin
BE	Bentonite
CU/BE	curcumin intercalated bentonite
ZnO@CU/BE	ZnO-decorated acid-activated bentonite-mediated curcumin extract
DPPH	1, 1-diphenyl-2-picrylhydrazil
PNPG	para-nitrophenyl α -glucopyranoside (PNPG)
ABTS	2,2'-azino-bis(3-ethylbenzothiazoline-6-sulphonic acid
DNSA	5-dinitrosalicylic acid
O ₂ ^{•-}	superoxide anion radical
•OH	hydroxyl radical
ROS	reactive oxygen species
LOI	Loss of ignition
ANOVA	analysis results of variance
XRD	X-ray diffraction pattern
SEM	Scanning electron microscope
HRTEM	Transmission electron microscope
FT-IR	Fourier-transform infrared

Author Contributions: Conceptualization, M.R.A., S.B., H.A.R.; methodology, M.H.S., M.R.A. and H.A.R.; Software, M.H.S., A.A.A. and L.M.A.; validation, M.R.A., S.B., H.A.R., A.A.A. and M.A.; formal analysis, M.H.S., A.A.A., M.A., L.M.A. and G.M.A.-T.; investigation, M.R.A., S.B., H.A.R., and A.A.A.; resources, A.A.A., M.H.S., L.M.A. and G.M.A.-T.; data curation, M.R.A., M.H.S., M.A., L.M.A. and G.M.A.-T.; writing—original draft preparation, M.R.A., M.H.S., M.A., A.A.A., S.B., H.A.R., L.M.A. and G.M.A.-T.; writing—review and editing, M.R.A., H.A.R., M.H.S., A.A.A., S.B., L.M.A. and G.M.A.-T.; visualization, M.R.A., H.A.R. and S.B.; supervision, M.R.A., S.B., A.A.A. and H.A.R.; project administration, M.R.A., H.A.R. and A.A.A.; funding acquisition, S.B. and H.A.R. All authors have read and agreed to the published version of the manuscript.

Funding: This research was funded by Deanship of Scientific Research at Imam Mohammad Ibn Saud Islamic University (IMSIU) grant number [RP-21-09-89].

Data Availability Statement: Data are available upon reasonable, by the Corresponding Authors.

Acknowledgments: The authors extend their appreciation to the Deanship of Scientific Research at Imam Mohammad Ibn Saud Islamic University (IMSIU) for funding and supporting this work through the Research Partnership Program no. (RP-21-09-89).

Conflicts of Interest: The authors declare no conflict of interest.

References

- Arvanag, F.M.; Bayrami, A.; Habibi-Yangjeh, A.; Pourn, S.R. A comprehensive study on antidiabetic and antibacterial activities of ZnO nanoparticles biosynthesized using *Silybum marianum* L seed extract. *Mater. Sci. Eng. C* **2019**, *97*, 397–405.
- Behl, T.; Kaur, I.; Sehgal, A.; Sharma, E.; Kumar, A.; Grover, M.; Bungau, S. Unfolding Nrf2 in diabetes mellitus. *Mol. Biol. Rep.* **2021**, *48*, 927–939.
- Billacura, M.P.; Cripps, M.J.; Hanna, K.; Sale, C.; Turner, M.D. β -alanine scavenging of free radicals protects mitochondrial function and enhances both insulin secretion and glucose uptake in cells under metabolic stress. *Adv. Redox Res.* **2022**, *6*, 100050.
- Hsu, W.H.; Chang, H.M.; Lee, Y.L.; Prasannan, A.; Hu, C.C.; Wang, J.S.; Lai, J.Y.; Yang, J.M.; Jebaranjitham, N.; Tsai, H.C. Biodegradable polymer-nanoclay composites as intestinal sleeve implants installed in digestive tract for obesity and type 2 diabetes treatment. *Mater. Sci. Eng. C* **2020**, *110*, 110676.
- Adersh, A.R.; Kulkarni, S.; Ghosh, P.; More, B.A.; Chopade, M.N. Gandhi, Surface defect rich ZnO quantum dots as antioxidant inhibiting α -amylase and α -glucosidase: A potential anti-diabetic nanomedicine. *J. Mater. Chem. B* **2015**, *3*, 4597–4606.
- Sagandira, C.R.; Khasipo, A.Z.; Sagandira, M.B.; Watts, P. An overview of the synthetic routes to essential oral anti-diabetes drugs. *Tetrahedron* **2021**, *96*, 132378.
- Robkhob, P.; Ghosh, S.; Bellare, J.; Jamdade, D.; Tang, I.M.; Thongmee, S. Effect of silver doping on antidiabetic and antioxidant potential of ZnO nanorods. *J. Trace Elem. Med. Biol.* **2020**, *58*, 126448.
- Asmat, U.; Abad, K.; Ismail, K. Diabetes mellitus and oxidative stress—A concise review. *Saudi Pharm. J.* **2016**, *24*, 547–553.
- Dedvisitsakul, P.; Watla-lad, K. Antioxidant activity and antidiabetic activities of Northern Thai indigenous edible plant extracts and their phytochemical constituents. *Heliyon* **2022**, *8*, e10740.
- Kim, M.S.; Jung, Y.S.; Jang, D.; Cho, C.H.; Lee, S.H.; Han, N.S.; Kim, D.O. Antioxidant capacity of 12 major soybean isoflavones and their bioavailability under simulated digestion and in human intestinal Caco-2 cells. *Food Chem.* **2022**, *374*, 131493.
- Chakraborty, S.; Amgai, B.; Bandyopadhyay, D.; Patel, N.; Hajra, A.; Narasimhan, B.; Rai, D.; Aggarwal, G.; Ghosh, R.K.; Yandrapalli, S.; et al. Acute myocardial infarction in the young with diabetes mellitus-national inpatient sample study with sex-based difference in outcomes. *Int. J. Cardiol.* **2021**, *326*, 35–41. [[CrossRef](#)]
- Feldman, E.L.; Callaghan, B.C.; Pop-Busui, R.; Zochodne, D.W.; Wright, D.E.; Bennett, D.L.; Bril, V.; Russell, J.W.; Viswanathan, V. Diabetic neuropathy. *Nat. Rev. Dis. Prim.* **2019**, *5*, 1–18.
- Frias, J.; Virdi, N.; Raja, P.; Kim, Y.; Savage, G.; Osterberg, L. Effectiveness of digital medicines to improve clinical outcomes in patients with uncontrolled hypertension and type 2 diabetes: Prospective, open-label, cluster-randomized pilot clinical trial. *J. Med. Internet Res.* **2017**, *19*, e7833. [[CrossRef](#)]
- Yilmazer-Musa, M.; Griffith, A.M.; Michels, A.J.; Schneider, E.; Frei, B. Grape seed and tea extracts and catechin 3-gallates are potent inhibitors of α -amylase and α -glucosidase activity. *J. Agric. Food Chem.* **2012**, *60*, 8924–8929. [[CrossRef](#)]
- Malik, A.R.; Sharif, S.; Shaheen, F.; Khalid, M.; Iqbal, Y.; Faisal, A.; Aziz, M.H.; Atif, M.; Ahmad, S.; Fakhar-e-Alam, M.; et al. Green synthesis of RGO-ZnO mediated *Ocimum basilicum* leaves extract nanocomposite for antioxidant, antibacterial, antidiabetic and photocatalytic activity. *J. Saudi Chem. Soc.* **2022**, *26*, 101438.
- Singh, T.A.; Sharma, A.; Tejwan, N.; Ghosh, N.; Das, J.; Sil, P.C. A state of the art review on the synthesis, antibacterial, antioxidant, antidiabetic and tissue regeneration activities of zinc oxide nanoparticles. *Adv. Colloid Interface Sci.* **2021**, *295*, 102495.
- Velsankar, K.; Venkatesan, A.; Muthumari, P.; Suganya, S.; Mohandoss, S.; Sudhahar, S. Green inspired synthesis of ZnO nanoparticles and its characterizations with biofilm, antioxidant, anti-inflammatory, and anti-diabetic activities. *J. Mol. Struct.* **2022**, *1255*, 132420.

18. Siddiqui, N.A.; Al-Yousef, H.M.; Alhowiriny, T.A.; Alam, P.; Hassan, W.H.; Amina, M.; Hussain, A.; Abdelaziz, S.; Abdallah, R.H. Concurrent analysis of bioactive triterpenes oleanolic acid and β -amyrin in antioxidant active fractions of *Hibiscus calyphyllus*, *Hibiscus deflersii* and *Hibiscus micranthus* grown in Saudi Arabia by applying validated HPTLC method. *Saudi Pharm. J.* **2018**, *26*, 266–273. [\[CrossRef\]](#)
19. Ahmed, Z.B.; Hefied, F.; Yousfi, M.; Demeyer, K.; Vander Heyden, Y. Study of the antioxidant activity of *Pistacia atlantica* Desf. Gall extracts and evaluation of the responsible compounds. *Biochem. Syst. Ecol.* **2022**, *100*, 104358.
20. Hajra, D.; Paul, S. Study of glucose uptake enhancing potential of fenugreek (*Trigonella foenum graecum*) leaves extract on 3T3 L1 cells line and evaluation of its antioxidant potential. *Pharmacogn. Res.* **2018**, *10*, 347–353.
21. Haritha, V.; Gowri, S.; Janarthanan, B.; Faiyazuddin, M.; Karthikeyan, C.; Sharmila, S. Biogenic synthesis of Nickel Oxide Nanoparticles using *Averrhoa bilimbi* and Investigation of its Antibacterial, Antidiabetic and Cytotoxic properties. *Inorg. Chem. Commun.* **2022**, *144*, 109930. [\[CrossRef\]](#)
22. Noohpisheh, Z.; Amiri, H.; Farhadi, S.; Mohammadi-Gholami, A. Green synthesis of Ag-ZnO nanocomposites using *Trigonella foenum-graecum* leaf extract and their antibacterial, antifungal, antioxidant and photocatalytic properties. *Spectrochim. Acta Part A Mol. Biomol. Spectrosc.* **2020**, *240*, 118595. [\[CrossRef\]](#)
23. Ansari, A.; Ali, A.; Khan, N.; Umar, M.S.; Owais, M. Synthesis of steroidal dihydropyrazole derivatives using green ZnO NPs and evaluation of their anticancer and antioxidant activity. *Steroids* **2022**, *188*, 109113. [\[CrossRef\]](#)
24. Song, Y.; Yang, F.; Ma, M.; Kang, Y.; Hui, A.; Quan, Z.; Wang, A. Green synthesized Se-ZnO/attapulgitite nanocomposites using Aloe vera leaf extract: Characterization, antibacterial and antioxidant activities. *LWT* **2022**, *165*, 113762. [\[CrossRef\]](#)
25. Sharma, A.; Nagraik, R.; Sharma, S.; Sharma, G.; Pandey, S.; Azizov, S.; Chauhan, P.K.; Kumar, D. Green synthesis of ZnO nanoparticles using *Ficus palmata*: Antioxidant, antibacterial and antidiabetic studies. *Results Chem.* **2022**, *4*, 100509. [\[CrossRef\]](#)
26. Yusof, N.A.A.; Zain, N.M.; Pauzi, N. Synthesis of ZnO nanoparticles with chitosan as stabilizing agent and their antibacterial properties against Gram-positive and Gram-negative bacteria. *Int. J. Biol. Macromol.* **2019**, *124*, 1132–1136. [\[CrossRef\]](#)
27. Prasad, S.; Lall, R. Zinc-curcumin based complexes in health and diseases: An approach in chemopreventive and therapeutic improvement. *J. Trace Elem. Med. Biol.* **2022**, *73*, 127023. [\[CrossRef\]](#)
28. Meer, B.; Andleeb, A.; Iqbal, J.; Ashraf, H.; Meer, K.; Ali, J.S.; Drouet, S.; Anjum, S.; Mehmood, A.; Khan, T.; et al. Bio-Assisted Synthesis and Characterization of Zinc Oxide Nanoparticles from *Lepidium Sativum* and Their Potent Antioxidant, Antibacterial and Anticancer Activities. *Biomolecules* **2022**, *12*, 855. [\[CrossRef\]](#)
29. Abukhadra, M.R.; AlHammadi, A.A.; Khim, J.S.; Ajarem, J.S.; Allam, A.A. Enhanced decontamination of Levofloxacin residuals from water using recycled glass based a green zinc oxide/mesoporous silica nanocomposite; adsorption and advanced oxidation studies. *J. Clean. Prod.* **2022**, *356*, 131836. [\[CrossRef\]](#)
30. Deng, J.; Wang, J.; Hu, H.; Hong, J.; Yang, L.; Zhou, H.; Xu, D. Application of mesoporous calcium silicate nanoparticles as a potential SD carrier to improve the solubility of curcumin. *J. Dispers. Sci. Technol.* **2022**, 1–9. [\[CrossRef\]](#)
31. Kour, P.; Afzal, S.; Gani, A.; Zargar, M.I.; Tak, U.N.; Rashid, S.; Dar, A.A. Effect of nanoemulsion-loaded hybrid biopolymeric hydrogel beads on the release kinetics, antioxidant potential and antibacterial activity of encapsulated curcumin. *Food Chem.* **2022**, *376*, 131925. [\[CrossRef\]](#)
32. Yixuan, L.; Qaria, M.A.; Sivasamy, S.; Jianzhong, S.; Daochen, Z. Curcumin production and bioavailability: A comprehensive review of curcumin extraction, synthesis, biotransformation and delivery systems. *Ind. Crops Prod.* **2021**, *172*, 114050. [\[CrossRef\]](#)
33. Khansili, N.; Krishna, P.M. Curcumin functionalized TiO₂ modified bentonite clay nanostructure for colorimetric Aflatoxin B1 detection in peanut and corn. *Sens. Bio-Sens. Res.* **2022**, *35*, 100480. [\[CrossRef\]](#)
34. Prasad, S.; DuBourdieu, D.; Srivastava, A.; Kumar, P.; Lall, R. Metal–Curcumin Complexes in Therapeutics: An Approach to Enhance Pharmacological Effects of Curcumin. *Int. J. Mol. Sci.* **2021**, *22*, 7094. [\[CrossRef\]](#)
35. Bernardo, A.; Plumitallo, C.; De Nuccio, C.; Visentin, S.; Minghetti, L. Curcumin promotes oligodendrocyte differentiation and their protection against TNF- α through the activation of the nuclear receptor PPAR- γ . *Sci. Rep.* **2021**, *11*, 1–13. [\[CrossRef\]](#)
36. Abukhadra, M.R.; Adlii, A.; El-Sherbeeny, A.M.; Soliman, A.T.A.; Abd Elatty, E. Promoting the decontamination of different types of water pollutants (Cd²⁺, safranin dye, and phosphate) using a novel structure of exfoliated bentonite admixed with cellulose nanofiber. *J. Environ. Manag.* **2020**, *273*, 111130. [\[CrossRef\]](#)
37. Wasim, M.; Shi, F.; Liu, J.; Zhang, H.; Zhu, K.; Tian, Z. Synthesis and characterization of curcumin/MMT-clay-treated bacterial cellulose as an antistatic and ultraviolet-resistive bioscaffold. *J. Polym. Res.* **2022**, *29*, 423. [\[CrossRef\]](#)
38. Mohammadhosseini, S.; Al-Musawi, T.J.; Romero Parra, R.M.; Qutob, M.; Gatea, M.A.; Ganji, F.; Balarak, D. UV and Visible Light Induced Photodegradation of Reactive Red 198 Dye and Textile Factory Wastewater on Fe₂O₃/Bentonite/TiO₂ Nanocomposite. *Minerals* **2022**, *12*, 1417. [\[CrossRef\]](#)
39. Tong, L.; Liang, T.; Tian, Y.; Zhang, Q.; Pan, Y. Research progress on treatment of mine wastewater by bentonite composite. *Arab. J. Geosci.* **2022**, *15*, 681. [\[CrossRef\]](#)
40. Kitture, R.; Ghosh, S.; More, P.A.; Gaware, S.; Datar, S.; Chopade, B.A.; Kale, S.N. Curcumin-loaded, self-assembled aloevera template for superior antioxidant activity and trans-membrane drug release. *J. Nanosci. Nanotechnol.* **2015**, *15*, 4039–4045. [\[CrossRef\]](#)
41. Dappula, S.S.; Kandrakonda, Y.R.; Shaik, J.B.; Mothukuru, S.L.; Lebaka, V.R.; Mannarapu, M.; Amooru, G.D. Biosynthesis of zinc oxide nanoparticles using aqueous extract of *Andrographis alata*: Characterization, optimization and assessment of their antibacterial, antioxidant, antidiabetic and anti-Alzheimer's properties. *J. Mol. Struct.* **2023**, *1273*, 134264. [\[CrossRef\]](#)

42. Sanap, S.P.; Ghosh, S.; Jabgunde, A.M.; Pinjari, R.V.; Gejji, S.P.; Singh, S.; Chopade, B.A.; Dhavale, D.D. Synthesis, computational study and glycosidase inhibitory activity of polyhydroxylated conidine alkaloids—A bicyclic iminosugar. *Org. Biomol. Chem.* **2010**, *8*, 3307–3315. [[CrossRef](#)]
43. Lawande, P.P.; Sontakke, V.A.; Kumbhar, N.M.; Bhagwat, T.R.; Ghosh, S.; Shinde, V.S. Polyhydroxylated azetidine iminosugars: Synthesis, glycosidase inhibitory activity and molecular docking studies. *Bioorganic Med. Chem. Lett.* **2017**, *27*, 5291–5295. [[CrossRef](#)]
44. Koksall, E.; Afsin, B.; Tabak, A.; Caglar, B. Butylamine-resadiye bentonite composite characterization. *Spectrosc. Lett.* **2020**, *53*, 745–750. [[CrossRef](#)]
45. Darmawan, M.A.; Muhammad, B.Z.; Harahap, A.F.P.; Ramadhan, M.Y.A.; Sahlan, M.; Supriyadi, T.; Abd-Aziz, S.; Gozan, M. Reduction of the acidity and peroxide numbers of tengkawang butter (*Shorea stenoptera*) using thermal and acid activated bentonites. *Heliyon* **2020**, *6*, e05742. [[CrossRef](#)]
46. Nagahashi, E.; Ogata, F.; Saenjum, C.; Nakamura, T.; Kawasaki, N. Preparation and Characterization of Acid-Activated Bentonite with Binary Acid Solution and Its Use in Decreasing Electrical Conductivity of Tap Water. *Minerals* **2021**, *11*, 815. [[CrossRef](#)]
47. Khatun, B.; Banik, N.; Hussain, A.; Ramteke, A.; Maji, T. Genipin crosslinked curcumin loaded chitosan/montmorillonite K-10 (MMT) nanoparticles for controlled drug delivery applications. *J. Microencapsul.* **2018**, *35*, 439–453. [[CrossRef](#)]
48. Abdel Salam, M.; Abukhadra, M.R.; Adlii, A. Insight into the adsorption and photocatalytic behaviors of an organo-bentonite/Co₃O₄ green nanocomposite for malachite green synthetic dye and Cr (VI) metal ions: Application and mechanisms. *ACS Omega* **2020**, *5*, 2766–2778. [[CrossRef](#)]
49. Abdel Salam, M.; Mokhtar, M.; Albukhari, S.M.; Baamer, D.F.; Palmisano, L.; Jaremko, M.; Abukhadra, M.R. Synthesis and Characterization of Green ZnO@ polyaniline/Bentonite Tripartite Structure (G. Zn@ PN/BE) as Adsorbent for As (V) Ions: Integration, Steric, and Energetic Properties. *Polymers* **2022**, *14*, 2329. [[CrossRef](#)]
50. Dardir, F.M.; Mohamed, A.S.; Abukhadra, M.R.; Ahmed, E.A.; Soliman, M.F. Cosmetic and pharmaceutical qualifications of Egyptian bentonite and its suitability as drug carrier for Praziquantel drug. *Eur. J. Pharm. Sci.* **2018**, *115*, 320–329. [[CrossRef](#)]
51. Dhall, A.; Self, W. Cerium oxide nanoparticles: A brief review of their synthesis methods and biomedical applications. *Antioxidants* **2018**, *7*, 97. [[CrossRef](#)]
52. Parul, R.; Kundu, S.K.; Saha, P. In vitro nitric oxide scavenging activity of methanol extracts of three Bangladeshi medicinal plants. *Pharma Innov.* **2013**, *1*, 83.
53. Sharpe, E.; Andreescu, D.; Andreescu, S. Artificial nanoparticle antioxidants. In *Oxidative Stress: Diagnostics, Prevention, and Therapy*; American Chemical Society: Washington, DC, USA, 2011; pp. 235–253.
54. Saad, A.M.; Abukhadra, M.R.; Ahmed, S.A.K.; Elzanaty, A.M.; Mady, A.H.; Betiha, M.A.; Shim, J.J.; Rabie, A.M. Photocatalytic degradation of malachite green dye using chitosan supported ZnO and Ce–ZnO nano-flowers under visible light. *J. Environ. Manag.* **2020**, *258*, 110043. [[CrossRef](#)]
55. Wang, Z.J.; Xu, J.J.; Ji, F.Y.; Luo, S.Z.; Li, X.J.; Mu, D.D.; Jiang, S.T.; Zheng, Z. Fabrication and characterization of soy β -conglycinin-dextran-polyphenol nanocomplexes: Improvement on the antioxidant activity and sustained-release property of curcumin. *Food Chem.* **2022**, *395*, 133562. [[CrossRef](#)]
56. Ayodhya, D.; Veerabhadram, G. Facile thermal fabrication of CuO nanoparticles from Cu (II)-Schiff base complexes and its catalytic reduction of 4-nitrophenol, antioxidant, and antimicrobial studies. *Chem. Data Collect.* **2019**, *23*, 100259. [[CrossRef](#)]
57. Sudha, A.; Jeyakanthan, J.; Srinivasan, P. Green synthesis of silver nanoparticles using Lippia nodiflora aerial extract and evaluation of their antioxidant, antibacterial and cytotoxic effects. *Resour. Effic. Technol.* **2017**, *3*, 506–515. [[CrossRef](#)]
58. Ramachandiran, D.; Elangovan, M.; Rajesh, K. Structural, optical, biological and photocatalytic activities of platinum nanoparticles using salixtetrasperma leaf extract via hydrothermal and ultrasonic methods. *Optik* **2021**, *244*, 167494. [[CrossRef](#)]
59. Hosny, M.; Fawzy, M.; El-Badry, Y.A.; Hussein, E.E.; Eltaweil, A.S. Plant-assisted synthesis of gold nanoparticles for photocatalytic, anticancer, and antioxidant applications. *J. Saudi Chem. Soc.* **2022**, *26*, 101419. [[CrossRef](#)]
60. Liu, Y.; Ying, D.; Cai, Y.; Le, X. Improved antioxidant activity and physicochemical properties of curcumin by adding ovalbumin and its structural characterization. *Food Hydrocoll.* **2017**, *72*, 304–311. [[CrossRef](#)]
61. Oun, A.A.; Bae, A.Y.; Shin, G.H.; Park, M.K.; Kim, J.T. Comparative study of oregano essential oil encapsulated in halloysite nanotubes and diatomaceous earth as antimicrobial and antioxidant composites. *Appl. Clay Sci.* **2022**, *224*, 106522. [[CrossRef](#)]
62. Mohammadian, M.; Salami, M.; Moghadam, M.; Amirsalehi, A.; Emam-Djomeh, Z. Mung bean protein as a promising biopolymeric vehicle for loading of curcumin: Structural characterization, antioxidant properties, and in vitro release kinetics. *J. Drug Deliv. Sci. Technol.* **2021**, *61*, 102148. [[CrossRef](#)]
63. Lin, D.; Xiao, L.; Qin, W.; Loy, D.A.; Wu, Z.; Chen, H.; Zhang, Q. Preparation, characterization and antioxidant properties of curcumin encapsulated chitosan/lignosulfonate micelles. *Carbohydr. Polym.* **2022**, *281*, 119080. [[CrossRef](#)]
64. Hamasaki, T.; Kashiwagi, T.; Imada, T.; Nakamichi, N.; Aramaki, S.; Toh, K.; Morisawa, S.; Shimakoshi, H.; Hisaeda, Y.; Shirahata, S. Kinetic analysis of superoxide anion radical-scavenging and hydroxyl radical-scavenging activities of platinum nanoparticles. *Langmuir* **2008**, *24*, 7354–7364. [[CrossRef](#)]
65. Xie, J.; Wang, N.; Dong, X.; Wang, C.; Du, Z.; Mei, L.; Yong, Y.; Huang, C.; Li, Y.; Gu, Z.; et al. Graphdiyne nanoparticles with high free radical scavenging activity for radiation protection. *ACS Appl. Mater. Interfaces* **2018**, *11*, 2579–2590. [[CrossRef](#)]
66. Shu, G.; Xu, D.; Xie, S.; Chang, L.J.; Liu, X.; Yang, J.; Li, Y.; Wang, X. The antioxidant, antibacterial, and infected wound healing effects of ZnO quantum dots-chitosan biocomposite. *Appl. Surf. Sci.* **2023**, *611*, 155727. [[CrossRef](#)]

67. Selvan, D.S.A.; Kumar, R.S.; Murugesan, S.; Shobana, S.; Rahiman, A.K. Antidiabetic activity of phytosynthesized Ag/CuO nanocomposites using *Murraya koenigii* and *Zingiber officinale* extracts. *J. Drug Deliv. Sci. Technol.* **2022**, *67*, 102838. [[CrossRef](#)]
68. Sabeena, G.; Rajadurai, S.; Manju, T.; Alhadlaq, H.A.; Mohan, R.; Annadurai, G.; Ahamed, M. In vitro antidiabetic and anti-inflammatory effects of Fe-doped CuO-rice husk silica (Fe-CuO-SiO₂) nanocomposites and their enhanced innate immunity in zebrafish. *J. King Saud Univ.-Sci.* **2022**, *34*, 102121. [[CrossRef](#)]
69. Vinotha, V.; Iswarya, A.; Thaya, R.; Govindarajan, M.; Alharbi, N.S.; Kadaikunnan, S.; Khaled, J.M.; Al-Anbr, M.N.; Vaseeharan, B. Synthesis of ZnO nanoparticles using insulin-rich leaf extract: Anti-diabetic, antibiofilm and anti-oxidant properties. *J. Photochem. Photobiol. B Biol.* **2019**, *197*, 111541. [[CrossRef](#)]
70. Rehana, D.; Mahendiran, D.; Kumar, R.S.; Rahiman, A.K. In vitro antioxidant and antidiabetic activities of zinc oxide nanoparticles synthesized using different plant extracts. *Bioprocess Biosyst. Eng.* **2017**, *40*, 943–957. [[CrossRef](#)]
71. Alkaladi, A.; Abdelazim, A.M.; Afifi, M. Antidiabetic activity of zinc oxide and silver nanoparticles on streptozotocin-induced diabetic rats. *Int. J. Mol. Sci.* **2014**, *15*, 2015–2023. [[CrossRef](#)]
72. Dhobale, S.; Thite, T.; Laware, S.L.; Rode, C.V.; Koppikar, S.J.; Ghanekar, R.K.; Kale, S.N. Zinc oxide nanoparticles as novel alpha-amylase inhibitors. *J. Appl. Phys.* **2008**, *104*, 094907. [[CrossRef](#)]

Disclaimer/Publisher's Note: The statements, opinions and data contained in all publications are solely those of the individual author(s) and contributor(s) and not of MDPI and/or the editor(s). MDPI and/or the editor(s) disclaim responsibility for any injury to people or property resulting from any ideas, methods, instructions or products referred to in the content.